Impact of crystalline anisotropy on the extrinsic spin Hall effect in ultrathin films

Christian Herschbach,[1] Dmitry V. Fedorov,[2] Martin Gradhand,[3,*] and Ingrid Mertig[1,4]

[1] *Institute of Physics, Martin Luther University Halle-Wittenberg, 06099 Halle, Germany*
[2] *Department of Physics and Materials Science, University of Luxembourg, L-1511 Luxembourg, Luxembourg*
[3] *H. H. Wills Physics Laboratory, University of Bristol, Bristol BS8 1TL, United Kingdom*
[4] *Max Planck Institute of Microstructure Physics, Weinberg 2, 06120 Halle, Germany*

An efficient conversion of a charge current into a spin current is a crucial point for application of the spin Hall effect in practical spintronic devices. Recently, we revealed that this goal can be achieved by using ultrathin fcc (111) and (001) noble metal films doped with Bi impurities which possess spin Hall angles up to 80%. Here, we show that the effect can be further amplified in monolayer films with a strong crystalline anisotropy. This is demonstrated by considering noble metal films with fcc (110) geometry. Our theoretical study predicts related spin Hall angles exceeding 100% especially when the crystalline anisotropy is increased, which tunes the Fermi surface topology.

PACS numbers: 71.15.Rf,72.25.Ba,75.76.+j,85.75.-d

The spin Hall effect (SHE)[1,2] is the key phenomenon for the creation of pure spin currents in nonmagnetic materials. For effective technological applications the spin Hall angle (SHA), the ratio between the transverse spin conductivity, i.e. the spin Hall conductivity (SHC), and the longitudinal charge conductivity, needs to be maximized. As there is no natural limit for the SHA, since it is solely a ratio between two conductivities, SHAs larger than 100% can be achieved. For topological insulators, such large values were reported recently[3–6]. There is a certain progress in increasing the efficiency of the SHE for metals[7–10] as well. However, to the best of our knowledge, SHAs for metals above 100% have not been discussed in the literature to date. The purpose of this work is to highlight a promising route of achieving such a strong SHE in metallic systems.

There are several routes to increase the charge-to-spin current conversion efficiency in metals that are associated with the underlying microscopic processes contributing to the SHE[11]. The so-called *intrinsic* mechanism, depending on the properties of the host material itself, is especially pronounced when the intrinsic spin-orbit coupling is strong. Hence, Pt is one of the most famous materials used for spin Hall applications relying on the intrinsic contribution[12–14]. In addition, β-Ta[8,15] and β-W[7,16,17] show distinctly large spin Hall angles due to their reduced charge conductivity in the high-resistive β-phase. Alongside the intrinsic effect, there are two *extrinsic* contributions to the spin Hall conductivity caused by the skew-scattering and side-jump mechanism. They are strongly influenced by impurities[18–20], which gives many opportunities to manipulate the strength of the SHE[21–24]. As was shown in Ref. 25, skew scattering dominates over the side-jump mechanism in dilute alloys since the former is inversely proportional to the impurity concentration. Therefore, we exploit the opportunity to maximize the SHE by means of the skew-scattering contribution.

Important research in this direction[26–30] revealed Bi impurities as strong p scatterers in noble metals to cause considerably large SHAs. The corresponding theoretical investigation predicted the SHA of 8.1% for bulk Cu(Bi) alloy[26]. The existence of a *giant* SHE with the SHA of the order of 10% was confirmed experimentally for thin films of this material combination[27]. Further work indicated the importance of a reduced film thickness for the amplification of the SHE[28,29]. Up to now, this climaxed in the prediction of a *colossal* SHE, referring to SHAs of the order of 100%, for Bi-doped noble metal monolayer (ML) films[30].

A crucial point discussed along with the intrinsic spin and anomalous Hall effect is the crystalline anisotropy. Especially, the impact of magnetic anisotropy as well as structural anisotropy in non-cubic crystals was investigated[31–34]. Following this direction, we combine the outlined paths by investigating Bi-doped 1 ML noble metal films with a structural in-plane anisotropy for the case of (110) surface orientation. Moreover, we explore the effects of increased or decreased crystalline anisotropy on a microscopic level of understanding and finally achieve spin Hall angles exceeding 100%.

As mentioned above, our research focuses on the maximization of the SHA. For the spin quantization axis chosen along the z axis, this is defined as

$$\alpha = \frac{\sigma^s_{yx}}{\sigma_{xx}}\,. \tag{1}$$

Here, σ^s_{yx} is the SHC and σ_{xx} denotes the longitudinal charge conductivity for an electric field applied along the x direction. Both quantities are elements of the related charge and spin conductivity tensors

$$\underline{\sigma} = \begin{pmatrix} \sigma_{xx} & \sigma_{xy} \\ \sigma_{yx} & \sigma_{yy} \end{pmatrix} \quad \text{and} \quad \underline{\sigma}^s = \begin{pmatrix} \sigma^s_{xx} & \sigma^s_{xy} \\ \sigma^s_{yx} & \sigma^s_{yy} \end{pmatrix}, \tag{2}$$

which are written in their general form for two-dimensional (2D) systems in xy-plane. Similar to Ref. 35, the spin conductivity is given in units of the charge conductivity, to result in a dimensionless SHA. The definitions given by Eq. (2) can be simplified taking into account the symmetry of the system. In case of nonmagnetic crystals, the transverse components of the charge

conductivity as well as the longitudinal elements of the spin conductivity vanish: $\sigma_{yx} = \sigma_{xy} = \sigma^s_{xx} = \sigma^s_{yy} = 0$[36]. In addition, the symmetry of (001) and (111) films[30] leads to $\sigma_{xx} = \sigma_{yy}$ and $\sigma^s_{yx} = -\sigma^s_{xy}$ allowing for the SHA of Eq. (1) to be uniquely defined and widely used. However, for (110) films, the symmetry is reduced[36] and the conductivity tensors have the following general form

$$\underline{\sigma} = \begin{pmatrix} \sigma_{xx} & 0 \\ 0 & \sigma_{yy} \end{pmatrix} \quad \text{and} \quad \underline{\sigma}^s = \begin{pmatrix} 0 & \sigma^s_{xy} \\ \sigma^s_{yx} & 0 \end{pmatrix} . \tag{3}$$

In particular, the transverse components of the spin conductivity are independent of each other and may be different. Accordingly, the related SHA becomes an anisotropic quantity and, therefore, needs to be used in its generalized definition

$$\alpha^i_j = \frac{\sigma^s_{ij}}{\sigma_{jj}} , \qquad (i,j = \{x,y\}, i \neq j) . \tag{4}$$

Our computational scheme relies on the density functional theory using the local density approximation in the parametrization of Vosko, Wilk, and Nusair[37]. First, we solve the Dirac equation by means of the relativistic Korringa-Kohn-Rostoker (KKR) Green's function method[29,38,39]. Then, the transport calculations are performed based on the semiclassical approach. We solve the linearized Boltzmann equation for the mean free path[18,26,29]

$$\mathbf{\Lambda}_{\boldsymbol{k}} = \tau_{\boldsymbol{k}} \left(\mathbf{v}_{\boldsymbol{k}} + \sum_{\boldsymbol{k}'} P_{\boldsymbol{k}'\boldsymbol{k}} \mathbf{\Lambda}_{\boldsymbol{k}'} \right) \tag{5}$$

iteratively[40], for electron states forming the 2D Fermi surface represented by lines. Here, $\boldsymbol{k} = (\mathbf{k}, \nu)$ is a combination of the momentum $\mathbf{k}$ and the band index ν. For the band indexing, it is sufficient to distinguish between the two bands contributing to one degenerate band only present at the Fermi surface of the considered systems. These are no pure "spin-up" or "spin-down" states due to the used relativistic treatment. Consequently, we identify states with predominant "spin-up/down" character by $\nu = \pm$, respectively[39,41]. The quantities in Eq. (5) are the momentum relaxation time $\tau_{\boldsymbol{k}} = \left(\sum_{\boldsymbol{k}'} P_{\boldsymbol{k}\boldsymbol{k}'}\right)^{-1}$, the Fermi velocity $\mathbf{v}_{\boldsymbol{k}} = \frac{1}{\hbar} \frac{\partial E_{\mathbf{k}}}{\partial \boldsymbol{k}}$ and the transition probability $P_{\boldsymbol{k}\boldsymbol{k}'} \equiv P_{\boldsymbol{k}\to\boldsymbol{k}'}$ obtained from Fermi's golden rule [18,40]. Within the dilute limit, the transition probability is directly proportional[18] to the impurity concentration c, why all considered conductivities are scaling as c^{-1}. For the performed calculations, we fix c=1 at.%. The last term on the r.h.s. of Eq. (5) deserves special attention. It is the so-called scattering-in term which is equivalent to the vertex corrections that appear in the dilute impurity limit of the Kubo approach[25,42]. This term describes the rotation of the mean free path away from the direction of the Fermi velocity and is therefore responsible for the skew scattering. With the mean free path in hand, we construct the conductivity tensors in the low temperature limit as Fermi-line integrals[29,30] that describe

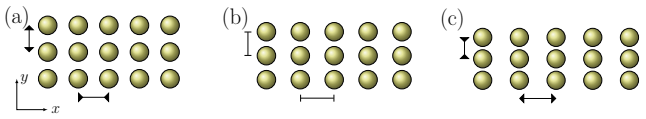

FIG. 1: (Color online) Illustration of the systems with different in-plane anisotropies: a) $x < x_0$, b) $x = x_0$, and c) $x > x_0$, where x_0 denotes the equilibrium distance. Case b) represents the usual (110) film and serves as a reference. To change the system's crystalline anisotropy, the interatomic distance in the y direction is changed so that the area of the Wigner-Seitz cell remains constant.

charge

$$\underline{\boldsymbol{\sigma}} = \frac{e^2}{\hbar(2\pi)^2 d} \oint\limits_{E_{\mathbf{k}}=E_F} \frac{\mathrm{d}l}{|\mathbf{v}_{\boldsymbol{k}}|} \mathbf{v}_{\boldsymbol{k}} \circ \mathbf{\Lambda}_{\boldsymbol{k}} \tag{6}$$

and spin conductivity

$$\underline{\boldsymbol{\sigma}}^s = \frac{e^2}{\hbar(2\pi)^2 d} \oint\limits_{E_{\mathbf{k}}=E_F} \frac{\mathrm{d}l}{|\mathbf{v}_{\boldsymbol{k}}|} s^z_{\boldsymbol{k}} \mathbf{v}_{\boldsymbol{k}} \circ \mathbf{\Lambda}_{\boldsymbol{k}} , \tag{7}$$

respectively. The corresponding film thickness is labelled by d and for the case of (110) monolayers of fcc crystals is given by $d = a\sqrt{2}/4$, where a is the lattice constant. Finally, s^z is the spin polarization[39,41] for the chosen spin quantization axis along the z direction.

We use the experimentally known lattice parameters to obtain the electronic structure of the considered 1 ML films. The large interatomic distance within the (110) plane is assumed to be 361.48 pm for Cu, 408.67 pm for Ag, and 407.82 pm for Au and points along the x direction. The distance in the y direction is shorter by a factor of $\frac{1}{\sqrt{2}}$, as shown in Fig. 1. In order to change the in-plane anisotropy, we simulate stress/strain. Namely, we increase or decrease the interatomic distance in the x direction and adjust the corresponding distance in the y direction so that the area of the Wigner-Seitz cell, the product of both, is kept constant. We label the respective situation by the lattice parameter in the x direction in comparison to the reference case $x = x_0$ shown in Fig. 1(b).

The SHA depends on two quantities, the longitudinal charge conductivity in the denominator as well as the transverse spin conductivity in the nominator of Eq. (4). First, we investigate the influence of changed lattice anisotropy on the longitudinal conductivity. To this end, we consider the ratio $\frac{x}{x_0}$ of the stressed/strained and reference interatomic distances in the x direction, for the range between 0.95 and 1.05. The longitudinal charge conductivities shown in Fig. 2(a) depend differently on the modified in-plane anisotropy. For all the investigated hosts, σ_{xx} decreases with increasing in-plane anisotropy, whereas σ_{yy} is almost constant for Cu, drastically increases for Ag and rises significantly in Au for the largest shown ratio $\frac{x}{x_0} = 1.05$ only.

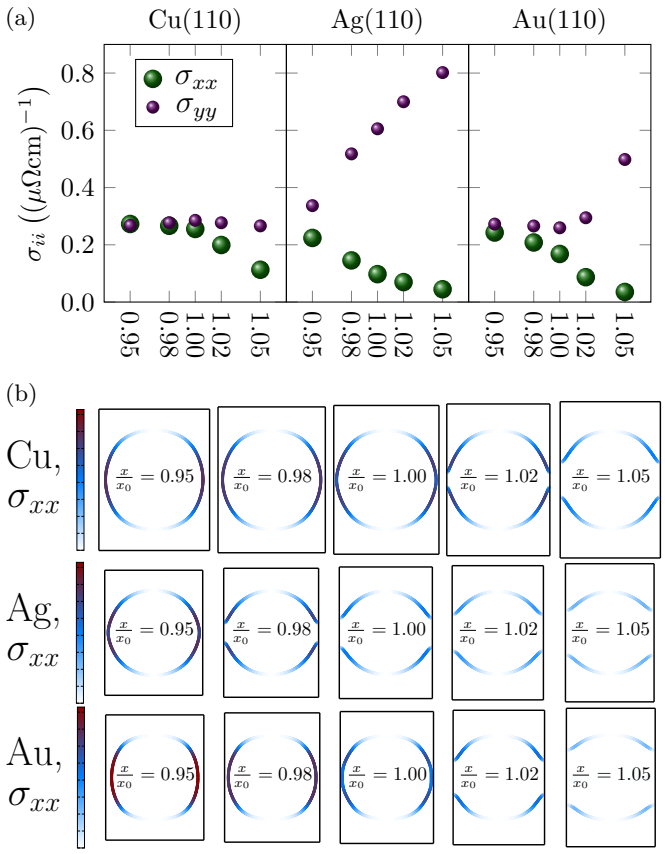

FIG. 2: (Color online) (a) Longitudinal charge conductivity due to Bi impurities in various 1 ML noble metal (110) films for different in-plane anisotropies $\frac{x}{x_0}$; (b) Distribution of **k**-dependent contributions (small [white, bright] to large [red, dark]) to the longitudinal charge conductivity σ_{xx} of 1 ML Cu, Ag, and Au(110) films for different in-plane anisotropies.

In order to realize the importance and relevance of the discussed results in terms of the strength of the SHE, it is essential to highlight that the longitudinal conductivities of the corresponding bulk systems are of the same order of magnitude. Namely, they are 0.22, 0.15, and $0.13\,(\mu\Omega\text{cm})^{-1}$ for Cu, Ag, and Au with substitutional Bi impurities[43]. In contrast to that, the transverse spin conductivities of the bulk Cu(Bi), Ag(Bi), and Au(Bi) alloys are 0.018, 0.014, and 0.002, respectively, being at least one order of magnitude smaller than in the considered 1ML (110) films (see Fig. 3). Accordingly, the increased SHA of the films, in comparison to the corresponding bulk systems, is mostly caused by a larger transverse spin current. However, a further enhancement of the SHA can be achieved by a decrease of longitudinal conductivities. Therefore, we analyze the behavior of σ_{xx} in some more detail.

Despite some general similarity, the three hosts show rather distinct features in the dependence of the longitudinal conductivity on crystalline anisotropy. In case of Cu and Au, σ_{xx} has a plateau for $x \leq x_0$ and an accompanied drop towards $\frac{x}{x_0} = 1.05$. A slightly different trend is visible for Ag with a steep slope appearing for $x < x_0$ which mildly levels off for $x > x_0$. Figure 2(b) illustrates the origin of these features. It shows the **k**-dependent integrand of Eq. (6) summed up over both spin channels. We present it in arbitrary units focusing on its relative contribution to the integral value. For instance, let us consider the Cu host in detail. For the reference situation $\frac{x}{x_0} = 1.00$, the main contributions originate from states in the $\pm k_x$ direction. Since the Fermi velocity is normal to the Fermi line, its v_x component is maximal there and vanishes for states with $k_x = 0$. For a decreased in-plane anisotropy, $x < x_0$, the 2D Brillouin zone (BZ) becomes larger/smaller in x/y direction without any change of the topology for the 2D Fermi surface. With increasing in-plane anisotropy, $x > x_0$, the Fermi surface touches the BZ boundary and a Lifshitz transition leads to the disappearance of states with velocities in the $\pm x$ direction. Consequently, they do not contribute to the longitudinal conductivity which therefore decreases. The same explanation holds for Au, where the Fermi surface touches the BZ boundary between $\frac{x}{x_0} = 1.00$ and $\frac{x}{x_0} = 1.02$ as well. In contrast to that, the corresponding process for Ag appears between 0.95 and 0.98. This leads to the steady decrease of σ_{xx} shown in the investigated regime of altered in-plane anisotropy. The behavior of σ_{yy}, especially its strong increase with increasing in-plane anisotropy in Ag, can be understood similarly. The touching point of the Fermi surface is shifted to positive/negative k_y direction for larger $\frac{x}{x_0}$ ratios. As a consequence, the Fermi lines become flatter with more states having larger v_y component which increases $\sigma_{yy} \propto v_y \Lambda_y$. On the other hand, for the considered geometry, a large in-plane anisotropy causes a decrease of σ_{xx} which is beneficial for large SHAs α_x^y.

Let us investigate the off-diagonal components of the spin conductivity with corresponding results shown in Fig. 3. In contrast to the longitudinal charge conductivity, the transverse spin conductivity is considerably (one order of magnitude) larger than the related bulk quantities[21]. As can be seen in Fig. 3(a), the absolute values of σ_{yx}^s and σ_{xy}^s are practically the same. Consequently, due to the fact that the smaller σ_{xx} should enhance the SHA, we discuss the associated σ_{yx}^s. Among the investigated systems, the created transverse spin current decreases with increasing in-plane anisotropy. The reason can be understood by considering Eq. (7). For the contribution from each twofold degenerate state **k** we can write

$$\sigma_{yx}^s(\mathbf{k}) \propto (v_\mathbf{k})_y \, (\mathbf{\Lambda}_\mathbf{k}^+ - \mathbf{\Lambda}_\mathbf{k}^-)_x \ , \tag{8}$$

where the negative sign of the spin polarization $s_\mathbf{k}^{z,-}$ of the relativistic "spin-down" state is taken into account explicitly. For the systems under investigation, the contribution is maximized for states with $k_x \approx 0$ (large v_y) having a large x component of the difference between $\mathbf{\Lambda}_\mathbf{k}^+$ and $\mathbf{\Lambda}_\mathbf{k}^-$. Figure 3(b) shows such spin-dependent mean free paths for some **k** points on the Fermi surface of two Ag films. Although the Fermi velocity of the mentioned states is very similar for the cases $\frac{x}{x_0} = 0.95$ and

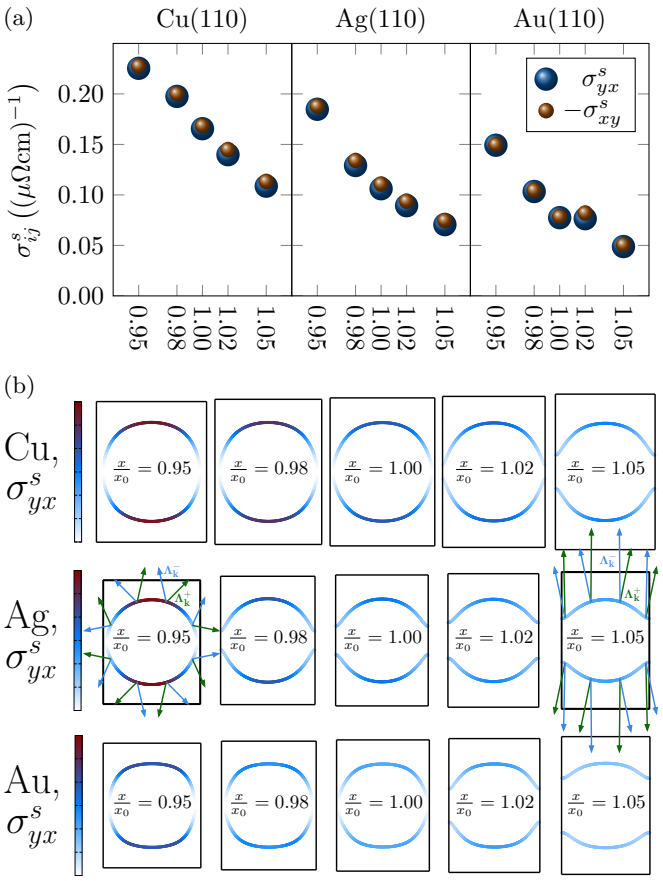

FIG. 3: (Color online) (a) Transverse spin conductivity due to Bi impurities in the considered 1 ML noble metal (110) films for different in-plane anisotropies $\frac{x}{x_0}$; (b) Distribution of $\mathbf{k}$-dependent contributions to the transverse spin conductivity σ^s_{yx} of 1 ML Cu, Ag, and Au(110) films for different in-plane anisotropies. For the two extreme Ag geometries, selected $\mathbf{k}$- and spin-dependent mean free paths $\mathbf{\Lambda}^{+/-}_{\mathbf{k}}$ are depicted.

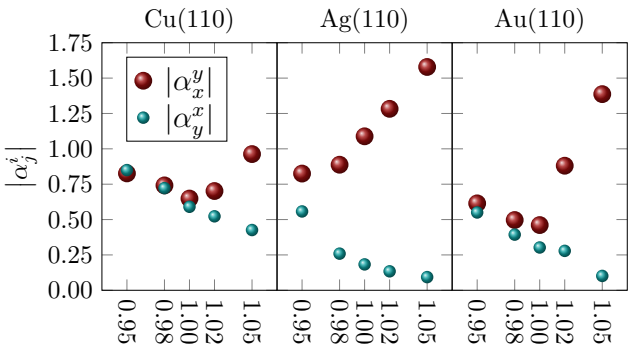

FIG. 4: (Color online) Absolute values of the SHAs due to Bi impurities in the considered 1 ML noble metal (110) films depending on different in-plane anisotropies.

$\frac{x}{x_0} = 1.05$, the angle between Λ^+ and Λ^- is smaller in the latter case. Consequently, the x component of the difference between the two mean free path vectors is reduced there which leads to smaller contributions to the transverse spin conductivity. As can be seen from Eq. (5), it is the scattering-in term, i.e. the action of $P_{\boldsymbol{k}'\boldsymbol{k}}$, which is responsible for the rotation of the mean free path away from the direction of the Fermi velocity. Accordingly, the associated efficiency of the scattering process w.r.t the creation of a transverse spin current is larger for $x < x_0$ among the considered systems.

Finally, we focus on the SHA which directly describes the charge-to-spin current conversion efficiency. The absolute values of the resulting SHAs for the investigated systems are shown in Fig. 4. As discussed above and shown by Figure 3(a), σ^s_{yx} and σ^s_{xy} have practically the same absolute values for all the considered systems. Consequently, strong differences between $|\alpha^y_x|$ and $|\alpha^x_y|$ originate from the different behavior of the longitudinal conductivities. While σ_{yy} is predominantly increasing (or almost constant in the case of Cu) we find that σ_{xx} is decreasing with an enhanced crystalline anisotropy. As a consequence, σ_{xx} becomes much smaller leading to the result that α^y_x is larger than α^x_y in almost all cases. The respective anisotropy-dependent trend is caused by the competition between longitudinal and transverse conductivities. The difference between the SHAs is most pronounced in case of Ag, where α^y_x exceeds 150% for the anisotropy factor $\frac{x}{x_0} = 1.05$. As indicated above, this is due to the fact that the 2D Fermi surface of Ag touches the BZ boundary already for a small value of in-plane anisotropy ($0.95 < \frac{x}{x_0} < 0.98$) in comparison to Cu and Au ($1.00 < \frac{x}{x_0} < 1.02$). Therefore, among the investigated systems, the 1 ML Ag(110) film grown on a proper substrate, providing it with a suitable crystalline anisotropy, would be the most promising candidate for practical devices employing the spin Hall effect. The obtained results suggest that a search for materials with the right Fermi surface anisotropy is enough to make predictions for a strong SHA. This is an interesting direction for future studies in this field.

In summary, we revealed that ultrathin noble metal films with in-plane anisotropy can possess an extremely strong spin Hall effect. This is demonstrated based on 1 ML fcc (110) Cu, Ag, and Au films doped with Bi impurities. In these systems, the spin Hall angle can exceed 100%. Such a strong effect is mostly caused by the stronger anisotropy of the longitudinal conductivity compared to the transverse spin conductivity, which are both reduced towards a longer in-plane lattice parameter. With the presented option of tuning the Fermi surface topology, the results of our study extend the pool of possibilities to enhance the spin Hall effect. Most importantly the principles uncovered here can be generalized beyond noble metals. Following our findings, metallic monolayer films with in-plane anisotropy, where bands are close to a Lifshitz transition essentially forming one-dimensional bands can be exploited to enhance the extrinsic spin Hall effect. Therefore, such materials could pave the way for building practical devices with efficient

charge-to-spin current conversion.

* Electronic address: m.gradhand@bristol.ac.uk

[1] M. Dyakonov and V. Perel, Physics Letters A **35**, 459 (1971).
[2] J. E. Hirsch, Phys. Rev. Lett. **83**, 1834 (1999).
[3] A. R. Mellnik, J. S. Lee, A. Richardella, J. L. Grab, P. J. Mintun, M. H. Fischer, A. Vaezi, A. Manchon, E.-A. Kim, N. Samarth, and D. C. Ralph, Nature **511**, 449 (2014).
[4] Y. Fan, P. Upadhyaya, X. Kou, M. Lang, S. Takei, Z. Wang, J. Tang, L. He, L.-T. Chang, M. Montazeri, G. Yu, W. Jiang, T. Nie, R. N. Schwartz, Y. Tserkovnyak, and K. L. Wang, Nature Materials **13**, 699 (2014).
[5] N. H. D. Khang, Y. Ueda, and P. N. Hai, Nature Materials **17**, 808 (2018).
[6] M. DC, R. Grassi, J.-Y. Chen, M. Jamali, D. Reifsnyder Hickey, D. Zhang, Z. Zhao, H. Li, P. Quarterman, Y. Lv, M. Li, A. Manchon, K. A. Mkhoyan, T. Low, and J.-P. Wang, Nature Materials **17**, 800 (2018).
[7] C.-F. Pai, L. Liu, Y. Li, H. W. Tseng, D. C. Ralph, and R. A. Buhrman, Applied Physics Letters **101**, 122404 (2012).
[8] L. Liu, C.-F. Pai, Y. Li, H. W. Tseng, D. C. Ralph, and R. A. Buhrman, Science **336**, 555 (2012).
[9] L. Zhu, D. C. Ralph, and R. A. Buhrman, Phys. Rev. Applied **10**, 031001 (2018).
[10] W.-B. Liao, T.-Y. Chen, Y. Ferrante, S. S. P. Parkin, and C.-F. Pai, physica status solidi (RRL) Rapid Research Letters **13**, 1900408 (2019).
[11] J. Sinova, S. O. Valenzuela, J. Wunderlich, C. H. Back, and T. Jungwirth, Rev. Mod. Phys. **87**, 1213 (2015).
[12] G. Y. Guo, S. Murakami, T.-W. Chen, and N. Nagaosa, Phys. Rev. Lett. **100**, 096401 (2008).
[13] M. Isasa, E. Villamor, L. E. Hueso, M. Gradhand, and F. Casanova, Phys. Rev. B **91**, 024402 (2015).
[14] M. Isasa, E. Villamor, L. E. Hueso, M. Gradhand, and F. Casanova, Phys. Rev. B **92**, 019905 (2015).
[15] R. Yu, B. F. Miao, L. Sun, Q. Liu, J. Du, P. Omelchenko, B. Heinrich, M. Wu, and H. F. Ding, Phys. Rev. Materials **2**, 074406 (2018).
[16] Q. Hao and G. Xiao, Phys. Rev. Appl. **3**, 034009 (2015).
[17] Q. Hao, W. Chen, and G. Xiao, Appl. Phys. Lett. **106**, 182403 (2015).
[18] M. Gradhand, D. V. Fedorov, P. Zahn, and I. Mertig, Phys. Rev. Lett. **104**, 186403 (2010).
[19] A. Fert and P. M. Levy, Phys. Rev. Lett. **106**, 157208 (2011).
[20] Y. Niimi, M. Morota, D. H. Wei, C. Deranlot, M. Basletic, A. Hamzic, A. Fert, and Y. Otani, Phys. Rev. Lett. **106**, 126601 (2011).
[21] M. Gradhand, D. V. Fedorov, P. Zahn, I. Mertig, Y. Otani, Y. Niimi, L. Vila, and A. Fert, SPIN **02**, 1250010 (2012).
[22] N. H. Long, P. Mavropoulos, B. Zimmermann, D. S. G. Bauer, S. Blügel, and Y. Mokrousov, Phys. Rev. B **90**, 064406 (2014).
[23] K. Chadova, S. Wimmer, H. Ebert, and D. Ködderitzsch, Phys. Rev. B **92**, 235142 (2015).
[24] B. Zimmermann, N. H. Long, P. Mavropoulos, S. Blügel, and Y. Mokrousov, Phys. Rev. B **94**, 060406 (2016).
[25] S. Lowitzer, M. Gradhand, D. Ködderitzsch, D. V. Fedorov, I. Mertig, and H. Ebert, Phys. Rev. Lett. **106**, 056601 (2011).
[26] M. Gradhand, D. V. Fedorov, P. Zahn, and I. Mertig, Phys. Rev. B **81**, 245109 (2010).
[27] Y. Niimi, Y. Kawanishi, D. H. Wei, C. Deranlot, H. X. Yang, M. Chshiev, T. Valet, A. Fert, and Y. Otani, Phys. Rev. Lett. **109**, 156602 (2012).
[28] B. Gu, I. Sugai, T. Ziman, G. Y. Guo, N. Nagaosa, T. Seki, K. Takanashi, and S. Maekawa, Phys. Rev. Lett. **105**, 216401 (2010).
[29] C. Herschbach, M. Gradhand, D. V. Fedorov, and I. Mertig, Phys. Rev. B **85**, 195133 (2012).
[30] C. Herschbach, D. V. Fedorov, M. Gradhand, and I. Mertig, Phys. Rev. B **90**, 180406(R) (2014).
[31] E. Roman, Y. Mokrousov, and I. Souza, Phys. Rev. Lett. **103**, 097203 (2009).
[32] E. M. Chudnovsky, Phys. Rev. B **80**, 153105 (2009).
[33] F. Freimuth, S. Blügel, and Y. Mokrousov, Phys. Rev. Lett. **105**, 246602 (2010).
[34] H. Zhang, S. Blügel, and Y. Mokrousov, Phys. Rev. B **84**, 024401 (2011).
[35] D. V. Fedorov, C. Herschbach, A. Johansson, S. Ostanin, I. Mertig, M. Gradhand, K. Chadova, D. Ködderitzsch, and H. Ebert, Phys. Rev. B **88**, 085116 (2013).
[36] M. Seemann, D. Ködderitzsch, S. Wimmer, and H. Ebert, Phys. Rev. B **92**, 155138 (2015).
[37] S. H. Vosko, L. Wilk, and M. Nusair, Can. J. Phys. **58**, 1200 (1980).
[38] J. Zabloudil, R. Hammerling, L. Szunyogh, and P. Weinberger, *Electron Scattering in Solid Matter.* (Springer-Verlag Berlin Heidelberg New York, 2005).
[39] M. Gradhand, M. Czerner, D. V. Fedorov, P. Zahn, B. Y. Yavorsky, L. Szunyogh, and I. Mertig, Phys. Rev. B **80**, 224413 (2009).
[40] I. Mertig, Rep. Prog. Phys. **62**, 237 (1999).
[41] F. Pientka, M. Gradhand, D. V. Fedorov, I. Mertig, and B. L. Györffy, Phys. Rev. B **86**, 054413 (2012).
[42] W. H. Butler, Phys. Rev. B **31**, 3260 (1985).
[43] M. Gradhand, D. V. Fedorov, P. Zahn, and I. Mertig, in *Trends in Magnetism*, Solid State Phenomena, Vol. 168 (Trans Tech Publications Ltd, 2011) pp. 27–30.